

Quark matter in Neutron Stars within the Field Correlator Method

S. Plumari^{a,b}, G. F. Burgio^c, V. Greco^{a,b}, and D. Zappalà^c

^a *Dipartimento di Fisica e Astronomia, Università di Catania, Via Santa Sofia 64, I-95123 Catania, Italia*

^b *INFN - Laboratori Nazionali del Sud, Via Santa Sofia 62, I-95125 Catania, Italia and*

^c *INFN Sezione di Catania, Via Santa Sofia 64, I-95123 Catania, Italia*

(Dated: February 25, 2022)

We discuss the appearance of quark matter in neutron star cores, focussing on the possibility that the recent observation of a very heavy neutron star could constrain free parameters of quark matter models. For that, we use the equation of state derived with the Field Correlator Method, extended to the zero temperature limit, whereas for the hadronic phase we use the equation of state obtained within both the non-relativistic and the relativistic Brueckner-Hartree-Fock many-body theory. We find a strong dependence of the maximum mass both on the value of the $q\bar{q}$ interaction V_1 , and on the gluon condensate G_2 , for which we introduce a dependence on the baryon chemical potential μ_B . We find that the maximum masses are consistent with the observational limit for not too small values of V_1 .

PACS numbers: 21.65.Qr, 26.60.Kp, 97.60.Jd, 12.38.Aw

I. INTRODUCTION

The appearance of quark matter in the interior of massive neutron stars (NS) is one of the mostly debated issues in the physics of these compact objects. Many equations of state (EoS) have been used to describe the interior of NS. If we consider only purely nucleonic degrees of freedom and the EoS is derived within microscopic approaches [1], it turns out that for the heaviest NS, close to the maximum mass (about two solar masses), the central particle density reaches values larger than $1/fm^3$. In this density range the nucleon cores (dimension ≈ 0.5 fm) start to touch each other, and it is hard to imagine that only nucleonic degrees of freedom can play a role. On the contrary, it can be expected that even before reaching these density values, the nucleons start to lose their identity, and quark degrees of freedom are excited at a macroscopic level.

Unfortunately it is not straightforward to predict the relevance of quark degrees of freedom in the interior of NS for the various physical observables, like cooling evolution, glitch characteristics, neutrino emissivity, and so on. The value of the maximum mass of NS is probably one of the physical quantities that is most sensitive to the presence of quark matter in NS. If the quark matter EoS is quite soft, the quark component is expected to appear in NS and to affect appreciably the maximum mass value. The recent observation of a large NS mass in PSR J0348+0432 with mass $M = 2.01 \pm 0.04 M_\odot$ [2] implies that the EoS of NS matter is stiff enough to keep the maximum mass at these large values. Purely nucleonic EoS are able to accommodate such large masses [1]. Since the presence of non-nucleonic degrees of freedom, like hyperons and quarks, tends usually to soften considerably the EoS with respect to purely nucleonic matter, thus lowering the mass value, their appearance would in

this case be incompatible with observations. The large value of the mass could then be explained only if both hyperonic and quark matter EoS are much stiffer than expected. Unfortunately, while the microscopic theory of the nucleonic EoS has reached a high degree of sophistication, the quark matter EoS is poorly known at zero temperature and at the high baryonic density appropriate for NS. One has, therefore, to rely on models of quark matter, which contain a high degree of uncertainty. The best one can do is to compare the predictions of different models and to estimate the uncertainty of the results for the NS matter as well as for the NS structure and mass. In this paper we will use two definite nucleonic EoS, which have been developed on the basis of the Brueckner-Hartree-Fock many-body theory for nuclear matter, and the Field Correlator Model (FCM) for the quark EoS [3], which in principle is able to cover the full temperature-chemical potential plane. The FCM EoS contains *ab initio* the property of confinement, which is expected to play a role as far as the stability of a neutron star is concerned [4], at variance with other models like, e.g., the Nambu–Jona-Lasinio model. In a previous paper [5] we analyzed the EoS of the quark matter in the FCM (for a review see [3]), and found that the model could be tested against NS observations, and these could seriously constrain the parameters used in the model. It was shown that this approach admits stable NS with gravitational masses slightly larger than $1.44 M_\odot$, thus providing numerical indications on some relevant physical quantities, such as the gluon condensate. In the present paper, we elaborate further on this idea, and explore the dependence of the model on the $q\bar{q}$ potential V_1 and, moreover, the dependence of the gluon condensate G_2 on the baryon chemical potential μ_B . The observation of a very large neutron star mass [2] can be used to put constraints on these two parameters.

This paper is organized as follows : in the next Section the FCM at finite temperature and density is briefly recalled, with an extensive discussion of the model param-

eters, while Sec.III contains some details of the EoS for the hadronic phase. In Sec.IV the hadron-quark phase transition is illustrated and the results of our analysis are presented in Sec.V. Finally, Sec.VI is devoted to the conclusions.

II. QUARK MATTER: EOS IN THE FIELD CORRELATOR METHOD

The approach based on the FCM provides a natural treatment of the dynamics of confinement in terms of the Color Electric (D^E and D_1^E) and Color Magnetic (D^H and D_1^H) Gaussian correlators, being the former one directly related to confinement, so that its vanishing above the critical temperature implies deconfinement [3]. The extension of the FCM to finite temperature T and chemical potential $\mu_q = 0$ gives analytical results in reasonable agreement with lattice data thus allowing to describe correctly the deconfinement phase transition [6–11]. In this work, we are interested in the physics of neutron stars, and therefore the extension of the FCM to finite values of the chemical potential [7, 8] allows to obtain the Equation of State of the quark-gluon matter in the range of baryon density typical of the neutron star interiors.

Within the FCM, the quark pressure for a single flavour is simply given by [7, 8, 11]

$$P_q/T^4 = \frac{1}{\pi^2} [\phi_\nu(\frac{\mu_q - V_1/2}{T}) + \phi_\nu(-\frac{\mu_q + V_1/2}{T})] \quad (1)$$

where

$$\phi_\nu(a) = \int_0^\infty du \frac{u^4}{\sqrt{u^2 + \nu^2}} \frac{1}{(\exp[\sqrt{u^2 + \nu^2} - a] + 1)}. \quad (2)$$

being $\nu = m_q/T$, and V_1 the large distance static $q\bar{q}$ potential:

$$V_1 = \int_0^{1/T} d\tau (1 - \tau T) \int_0^\infty d\chi \chi D_1^E(\sqrt{\chi^2 + \tau^2}) \quad (3)$$

The potential V_1 in Eq.(3) is assumed to be independent on the chemical potential, and this is partially supported by lattice simulations at very small chemical potential [8, 12]. We elaborate more on this point in the following subsection.

The EoS is completely specified once the gluon contribution is added to the quark pressure, i.e.

$$P_g/T^4 = \frac{8}{3\pi^2} \int_0^\infty d\chi \chi^3 \frac{1}{\exp(\chi + \frac{9V_1}{8T}) - 1} \quad (4)$$

and therefore

$$P_{qg} = P_g + \sum_{j=u,d,s} P_q^j + \Delta\epsilon_{vac} \quad (5)$$

where P_q and P_g^j are respectively given in Eq. (1) and (4), and

$$\Delta\epsilon_{vac} \approx -\frac{(11 - \frac{2}{3}N_f) G_2}{32 \cdot 2} \quad (6)$$

corresponds to the difference of the vacuum energy density in the two phases, being N_f the flavour number. G_2 is the gluon condensate whose numerical value, determined by the QCD sum rules, is known with large uncertainty [13]

$$G_2 = 0.012 \pm 0.006 \text{ GeV}^4 \quad (7)$$

Therefore the EoS in Eq.(5) essentially depends on two parameters, namely the quark-antiquark potential V_1 and the gluon condensate G_2 . In addition, at finite temperature and vanishing baryon density, a comparison with the available lattice calculations of the Wuppertal-Budapest, [14, 15], and hotQCD collaborations, [16–18], provides clear indications about the specific values of these parameters, and in particular their values at the critical temperature T_c . These estimates are related to the corresponding values of the parameters at $T = \mu_B = 0$ which, in turn, can be used as an input to study the EoS at $T = 0$ and finite μ_B .

A. The V_1 and G_2 parameters

In ref.[7] the EoS at zero baryon density has been derived, by explicitly assuming a temperature dependence of the gluon condensate G_2 as found in lattice simulations [19, 20], namely an almost constant $G_2(T)$ for $0 < T < T_c$, with a sudden drop around T_c to one half of its value, followed by the constant behavior $G_2(T) = G_2(T = 0)/2$, for $T > T_c$. In addition, an indication on the value of $V_1(T_c)$ has been extracted in [21], starting from the expression of the critical temperature obtained in [7, 8]

$$T_c = \frac{a_0 G_2^{1/4}}{2} \left(1 + \sqrt{1 + \frac{V_1(T_c)}{2a_0 G_2^{1/4}}} \right), \quad (8)$$

where $a_0 = (3\pi^2/768)^{1/4}$. In fact, once the values of G_2 and T_c are fixed, one immediately gets $V_1(T_c)$ from Eq. (8), and in ref. [21] it has been shown that, for $G_2(T = 0) = 0.012 \text{ GeV}^4$, the critical temperatures found in [14, 17], respectively $T_c = 147 \pm 5 \text{ MeV}$ and $T_c = 154 \pm 9 \text{ MeV}$, correspond to rather small values of V_1 ($V_1(T_c) \lesssim 0.15 \text{ GeV}$), while the optimum value indicated in [8], $V_1(T_c) = 0.5 \text{ GeV}$, reproduces those temperatures for small values of G_2 , i.e. $G_2 \simeq 0.004 \text{ GeV}^4$.

However, one should recall that Eq.(8) is not extremely accurate, being obtained by neglecting the hadron pressure at the transition, which in [8] is estimated as a 10% uncertainty. Hence a check of the EoS focused on the critical point $T = T_c$ only, could be too restrictive, as the numerical data on lattice cover a large temperature range

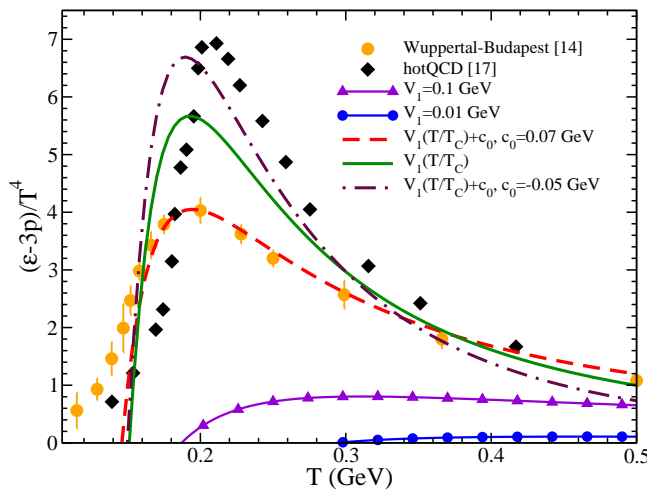


FIG. 1: The interaction measure $(\epsilon - 3p)/T^4$ as a function of the temperature as obtained in the FCM for three values of c_0 in Eq. (9) : $c_0 = 0.07, 0, -0.05$ GeV (respectively: dashed (red), solid (green) and dot-dashed (brown) curve), compared with the lattice data of ref. [15] (orange circles) and ref. [16] (black , diamonds).

above T_c . For that, we compare in Fig.1 the predictions of the FCM with the available lattice data around and above the critical temperature. In Fig.1 we concentrate on the interaction measure $(\epsilon - 3p)/T^4$, which is particularly significant because it depends both on the energy density and on the pressure of the system and shows, around the critical temperature, large deviations from zero, i.e. the value of the interaction measure of a free gas of massless particles. The predictions of the FCM are checked against the lattice data for different parametrizations of $V_1(T)$, and also for constant $V_1 = 0.01$ GeV and $V_1 = 0.1$ GeV. From Fig. 1 it is evident that these two constant values are too small, and higher values of V_1 must be considered. As suggested in ref.[8], we took

$$V_1(T) = c_0 + V_1 \left(\frac{T}{T_c} \right) = c_0 + 0.175 \left(1.35 \frac{T}{T_c} - 1 \right)^{-1} \text{ GeV} \quad (9)$$

with respectively $c_0 = 0.07, 0, -0.05$ GeV (corresponding to $V_1(T_c) = 0.57, 0.5, 0.45$ GeV). The results, displayed by the dashed (red), solid (green) and dot-dashed (brown) curves, show a much better agreement with the data, and in particular the dashed (red) curve with $V_1(T_c) = 0.57$ GeV gives a good fit to the data of [15], represented by full circles (orange), whereas $V_1(T_c) = 0.45$ is preferable for the data in [16] from the hotQCD collaboration, and shown as full diamonds (black). However, we warn that, more recently, also the hotQCD collaboration is converging toward a smaller peak for $(\epsilon - 3P)/T^4$ close to the Wuppertal-Budapest one as presented in [18].

This check shows that the analysis of the whole set of lattice data points toward a value of $V_1(T_c)$ around $0.5 - 0.6$ GeV while, as noticed above, the simple determination of the critical temperature T_c with reasonable values of G_2 would suggest smaller $V_1(T_c)$. The value of the potential at $T = 0$, which is essential, for the

study of NS structure, has been computed in [21] as a function of $V_1(T_c)$, by making use of Eq. (3), under the assumption of a temperature independent D_1^E in the region $0 < T < T_c$ [20], obtaining $V_1(T = 0) \simeq 0.8 \div 0.9$ GeV in correspondence of $V_1(T_c) = 0.5$ GeV.

It is important to notice that there is no direct relation of these values with the potential at finite μ_B . One would expect that an increasing baryon density could produce a screening effect that reduces the intensity of the quark-antiquark potential, and at large density the quark-quark interaction should become more and more relevant. In our analysis we choose to keep V_1 as a free parameter, and check what kind of indications on V_1 can be extracted from the determination of the maximum mass of neutron stars.

Let us now turn to the other parameter of the FCM model, namely the gluon condensate G_2 . As mentioned above, $G_2(T)$ at zero baryon density has been computed on lattice [19, 20] but, due to technical difficulties, analogous calculations in full QCD at large μ_B are precluded. Therefore we have to resort to different approaches to get some indications on the gluon condensate at $\mu_B \neq 0$. In particular, the QCD sum rules technique has been used to study some hadronic properties within a nuclear matter environment at $T = 0$ [22], and it has been found that the gluon condensate decreases linearly with the baryon density ρ_B (m_N indicates the neutron mass)

$$G_2(\rho_B) - G_2(\rho_B = 0) = -m_N \rho_B + O(\rho_B^2). \quad (10)$$

Further analysis [23, 24] show that the corrections to Eq. (10), even when including nonlinear effects, are substantially small and can be neglected for our purposes. According to this decreasing trend, the gluon condensate vanishes at some value of the baryon density and, as noticed in [24] one expects that a transition to the deconfined state should occur before reaching this point.

Once the behaviour of the condensate below the transition is given in Eq. (10), we still need to establish $G_2(\mu_B)$ at higher values of the baryon chemical potential to proceed in our analysis. Rather than following the simplest choice of taking an effective μ_B -independent G_2 , which was adopted in [5, 21], we prefer to retain Eq. (10) at lower densities and, at the same time, to follow the indications proposed in [25, 26] at higher density. In fact, in [25, 26] it is suggested that $G_2(\mu_B)$ in full three-color ($N_c = 3$) QCD, has the same qualitative behavior of the corresponding variable in two-color ($N_c = 2$) QCD. In this case many technical problems that affect the theory with $N_c = 3$, are absent and, in particular, the modification of the gluon condensate at finite chemical potential, namely the difference $f_{CS}(\mu) = G_2(\mu) - G_2(0)$, is computed from the energy momentum tensor of an effective chiral lagrangian with the following result:

$$f_{CS}(\mu) = 4f_\pi^2(\mu^2 - M^2) \left(1 - \frac{M^2}{\mu^2}\right) \quad (11)$$

where M is identified with the pion mass. Eq. (11) shows an initial decrease which, after reaching a minimum, is followed by a continuous growth. This trend is understood with the appearance of a weakly interacting gas of diquarks, whose pressure is negligible if compared to its energy density, which mostly comes from diquark rest mass. Accordingly, the gluon condensate, that is related to minus the trace energy momentum tensor, decreases with μ_B . Only at sufficiently large chemical potential the contribution of the diquarks on the pressure becomes approximately equal to energy density and the growth of the gluon condensate is observed. This result is also consistent with lattice calculations [27, 28] which can be carried out for $N_c = 2$. Finally in [25, 26] it is claimed that the color superconducting (CS) phase in the $N_c = 3$ theory should qualitatively reproduce the picture described above, and Eq. (11) does still hold, provided that in this case one takes $M \sim 2\Lambda_{QCD}$ and μ is identified with the quark chemical potential: $\mu = (1/3)\mu_B$.

Therefore we have put together the two curves of the gluon condensate at low and at high values of μ_B , given respectively in Eqs. (10) and (11), and selected $G_2(\mu_B)$ as the solid (red) line displayed in Fig. 2. More precisely, in Fig. 2 the dashed (green) and the dot-dashed (blue) lines respectively correspond to Eq. (10) (where $G_2(\rho_B)$ is reparametrized in terms of $G_2(\mu_B)$) and Eq. (11). Then, by crudely assuming that the transition point lies close to the intersection point of these two curves, we parametrized $G_2(\mu_B)$ through an effective analytic expression, the solid (red) line, which approximates Eq. (10) at low μ_B and Eq. (11) at higher μ_B . This analytic form avoids a discontinuity in the derivative of $G_2(\mu_B)$ at the intersection of the two curves that could produce unphysical features when computing the pressure or the energy density of the system. In Fig. 2 the value of the condensate at zero chemical potential is taken $G_2(\mu_B = 0) = 0.012 \text{ GeV}^4$.

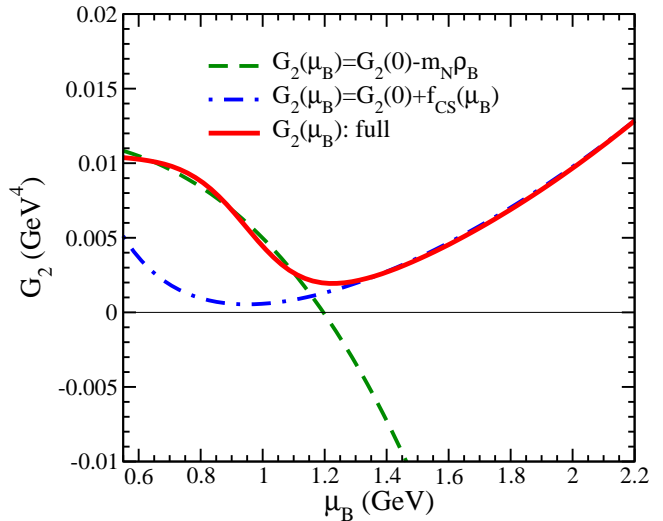


FIG. 2: $G_2(\mu_B)$ as obtained from Eq. (10) (green dashed) and Eq. (11) (blue dot-dashed) with $G_2(\mu_B = 0) = 0.012 \text{ GeV}^4$. The solid (red) line is the effective approximation used in our analysis. (see text).

III. HADRONIC PHASE: EOS IN THE BRUECKNER-BETHE-GOLDSTONE THEORY

In this section we remind briefly the BHF method for the nuclear matter EoS. This theoretical scheme is based on the Brueckner-Bethe-Goldstone (BBG) many-body theory, which is the linked cluster expansion of the energy per nucleon of nuclear matter (see Ref.[29], chapter 1 and references therein). In this many-body approach one systematically replaces the bare nucleon-nucleon (NN) interaction V by the Brueckner reaction matrix G , which is the solution of the Bethe-Goldstone equation

$$G(\rho; \omega) = V + V \sum_{k_a k_b} \frac{|k_a k_b\rangle Q \langle k_a k_b|}{\omega - e(k_a) - e(k_b)} G(\rho; \omega), \quad (12)$$

where ρ is the nucleon number density, ω is the starting energy, and $|k_a k_b\rangle Q \langle k_a k_b|$ is the Pauli operator. $e(k) = e(k; \rho) = \frac{\hbar^2}{2m} k^2 + U(k; \rho)$ is the single particle energy, and U is the single-particle potential,

$$U(k; \rho) = \sum_{k' \leq k_F} \langle k k' | G(\rho; e(k) + e(k')) | k k' \rangle_a \quad (13)$$

The subscript “ a ” indicates antisymmetrization of the matrix element. In the BHF approximation the energy per nucleon is

$$\frac{E}{A}(\rho) = \frac{3}{5} \frac{\hbar^2 k_F^2}{2m} + D_2, \quad (14)$$

$$D_2 = \frac{1}{2A} \sum_{k, k' \leq k_F} \langle k k' | G(\rho; e(k) + e(k')) | k k' \rangle_a \quad (15)$$

The nuclear EoS can be calculated with good accuracy in the Brueckner two hole-line approximation with the continuous choice for the single-particle potential, since the results in this scheme are quite close to the calculations which include also the three hole-line contribution. However, as it is well known, the non-relativistic calculations, based on purely two-body interactions, fail to reproduce the correct saturation point of symmetric nuclear matter and one needs to introduce three-body forces (TBFs). In our approach the TBF's are reduced to a density dependent two-body force by averaging over the position of the third particle [30]

In this work we choose the Argonne v_{18} nucleon-nucleon potential [31], supplemented by the so-called Urbana model [32] as three-body force. This allows to reproduce correctly the nuclear matter saturation point $\rho_0 \approx 0.17 \text{ fm}^{-3}$, $E/A \approx -16 \text{ MeV}$, and gives values of incompressibility and symmetry energy at saturation compatible with those extracted from phenomenology [33]. For completeness we will show results obtained with the relativistic counterpart, i.e. the Dirac-Brueckner-Hartree-Fock scheme [34] where the Bonn A potential is used as NN interaction. In the low density region ($\rho < 0.3 \text{ fm}^{-3}$), both BHF+TBF binding energies and DBHF calculations are very similar, whereas at higher densities the DBHF is slightly stiffer [1]. The discrepancy between the nonrelativistic and relativistic calculation can be easily understood by noticing that the DBHF treatment is equivalent to introducing in the nonrelativistic BHF the three-body force corresponding to the excitation of a nucleon-antinucleon pair, the so-called Z-diagram [35], which is repulsive at all densities. On the contrary, in the BHF treatment both attractive and repulsive three-body forces are introduced, and therefore a softer EoS is expected.

We remind that the BBG approach has been extended to the hyperonic sector in a fully self-consistent way [36, 37], by including the Σ^- and Λ hyperons, but in this paper we consider stellar matter as composed by neutrons, protons, and leptons in beta equilibrium [30]. The chemical potentials of each species are the fundamental input for solving the equations of chemical equilibrium, charge neutrality and baryon number conservation, yielding the equilibrium fractions of all species. Once the composition of the β -stable, charge neutral stellar matter is known, one can calculate the equation of state, i.e., the relation between pressure P and energy density ϵ as a function of the baryon density ρ . It can be easily obtained from the thermodynamical relation

$$P = -\frac{dE}{dV} = P_B + P_l \quad (16)$$

$$P_B = \rho^2 \frac{d(\epsilon_B/\rho)}{d\rho}, \quad P_l = \rho^2 \frac{d(\epsilon_l/\rho)}{d\rho} \quad (17)$$

with E the total energy and V the total volume. The total nucleonic energy density is obtained by adding the energy densities of each species ϵ_i . As far as leptons are concerned, at those high densities electrons are a free ul-

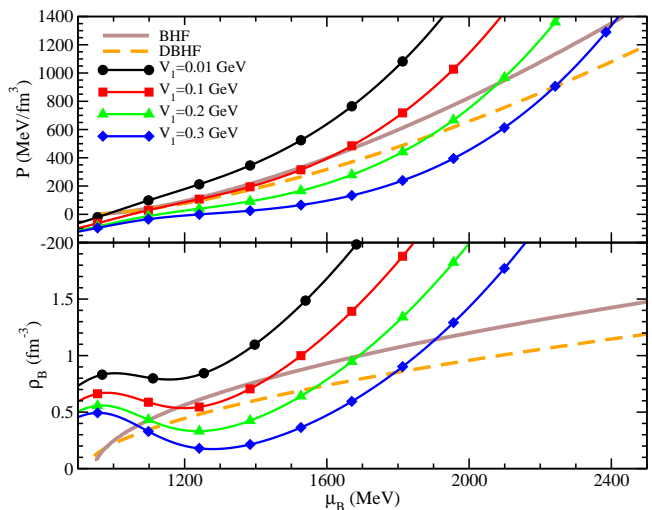


FIG. 3: The pressure P is displayed vs. the baryon chemical potential in the upper panel, whereas in the lower panel the baryon density is shown for different values of V_1 in the FCM model. The EoS's for the hadronic phase are represented by the solid line (brown color) for the BHF, and for the DBHF (dashed yellow curve) EoS's.

trarelativistic gas, whereas muons are relativistic. Hence their energy densities ϵ_l are well known from textbooks [38]. The numerical procedure has been often illustrated in papers and textbooks [38], and therefore it will not be repeated here.

IV. THE HADRON-QUARK PHASE TRANSITION

We are now able to compare the pressure of the two phases, namely the pressure in the hadronic phase given in Eqs.(16)-(17), and the quark pressure shown in Eq.(5). We adopt the simple Maxwell construction, by assuming a first order hadron-quark phase transition [39] in beta-stable matter. The more general Gibbs construction [40] is still affected by many theoretical uncertainties [41], and in any case the final mass-radius relation of massive neutron stars [42] is slightly affected.

We impose thermal, chemical, and mechanical equilibrium between the two phases. This implies that the phase coexistence is determined by a crossing point in the pressure vs. chemical potential plot, as shown in Fig. 3. There we display the pressure P (upper panel) and the baryon density (lower panel) as function of the baryon chemical potential μ_B for the baryonic and quark matter phases. The hadronic EoS's are plotted as solid (brown, BHF), and dashed (orange, DBHF) curves, whereas symbols are the results for quark matter EoS in the FCM and different choices of V_1 . We observe that the crossing points are significantly affected by the chosen value of the potential V_1 . Moreover, with increasing V_1 , the onset of the phase transition is shifted to larger chemical

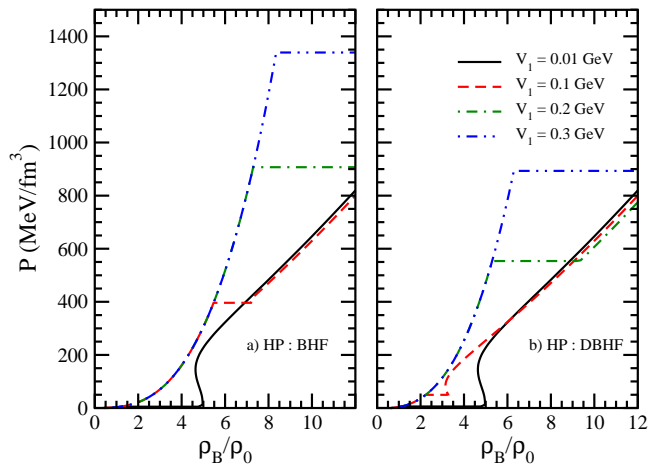


FIG. 4: The pressure P is displayed vs. the baryon density for different values of V_1 in the FCM model. In the left (right) panel calculations are shown when the BHF (DBHF) approach is used for the hadronic phase.

potentials. Hence, we expect that the neutron star will possess a thicker hadronic layer with increasing V_1 .

In Fig.4 we display the total EoS, i.e. the pressure as a function of the baryon density for the several cases discussed above. In particular we plot in the left panel the EoS obtained by using the BHF approach for the hadronic phase, whereas in the right panel calculations are shown for the case when the DBHF EoS is adopted. The several curves represent different choices of the $q\bar{q}$ potential V_1 . The plateaus are consequence of the Maxwell construction. Below the plateau, β -stable and charge neutral stellar matter is in the purely hadronic phase, whereas for density above the ones characterizing the plateau, the system is in the pure quark phase. The main features of the phase transition are displayed in Table I, where we report for a fixed hadronic EoS and several values of the $q\bar{q}$ potential V_1 , the baryonic chemical potential at the transition μ_B^{tr} , and the corresponding baryon density ρ^{tr} in units of the saturation density ρ_0 , and the gluon condensate G_2^{tr} . We see that, whenever the transition takes place at $\mu_B \lesssim 1.2$ GeV, i.e. below the minimum shown in Fig.2, the pressure P shows a kink as a function of the baryon density, and this is due to the particular parametric form of the gluon condensate G_2 shown in Fig.2. The presence of a kink gives unstable neutron stars configurations, as it will be shown in the next Section.

V. RESULTS AND DISCUSSION

The EoS is the fundamental input for solving the well-known hydrostatic equilibrium equations of Tolman, Oppenheimer, and Volkoff [38] for the pressure P and the

TABLE I: Properties of the hadron-quark phase transition.

	V_1 (GeV)	μ_B^{tr} (GeV)	ρ^{tr}/ρ_0	G_2^{tr} (GeV ⁴)
BHF	0.01	0.986	1.22	0.0048
	0.1	1.606	5.51	0.0046
	0.2	2.09	7.33	0.0109
	0.3	2.408	8.4	0.0165
DBHF	0.01	0.987	1.17	0.0047
	0.1	1.14	2.26	0.0023
	0.2	1.89	5.29	0.0079
	0.3	2.24	6.31	0.0165

enclosed mass m

$$\frac{dP(r)}{dr} = -\frac{Gm(r)\epsilon(r)}{r^2} \frac{\left[1 + \frac{P(r)}{\epsilon(r)}\right] \left[1 + \frac{4\pi r^3 P(r)}{m(r)}\right]}{1 - \frac{2Gm(r)}{r}} \quad (18)$$

$$\frac{dm(r)}{dr} = 4\pi r^2 \epsilon(r), \quad (19)$$

being ϵ the total energy density (G is the gravitational constant). For a chosen central value of the energy density, the numerical integration of Eqs. (18) and (19) provides the mass-radius relation. For the description of the neutron star crust, we have joined the equations of state above described with the ones by Negele & Vautherin [43] in the medium-density regime, and the ones by Baym, Pethick, & Sutherland [44] for the outer crust ($\rho < 0.001$ fm⁻³), and Feynman, Metropolis, & Teller [45]. In Fig.5 we display the gravitational mass (in units of solar mass $M_\odot = 2 \times 10^{33}$ g) as a function of the radius R (left panel) and the corresponding central baryon density, normalized with respect to the saturation value (right panel). Stellar configurations have been obtained using the BHF EoS for the hadronic phase. The orange band represents the recently observed neutron star PSR J0348+0432 with mass $M = 2.01 \pm 0.04 M_\odot$ [2]. We have marked the stable configurations by thick lines, whereas full symbols denote the maximum mass. Unstable configurations are displayed by thin lines. Among the unstable configurations, we signal those characterized by increasing mass and decreasing central density, which are related to the appearance of the kink in the EoS, as anticipated in Sect.IV. In Table II we display the values characterizing the maximum mass, i.e. the central density (in units of ρ_0) and the corresponding value of the gluon condensate G_2 whenever the core contains quark matter. Those configurations are stable and the mass values are denoted by an asterisk. We see that the maximum value spans over a range between 1.69 and 2.03 solar masses, depending on the value of the $q\bar{q}$ potential V_1 . However, the observational data indicate that values of V_1 as small as 0.01 GeV are excluded, and that values of about 0.1 GeV are only marginally compatible with the observational data. Larger values of V_1 produce increasing maximum masses, but the stable stars are in the purely hadronic phase. We found that $V_1 \approx 0.095$ GeV

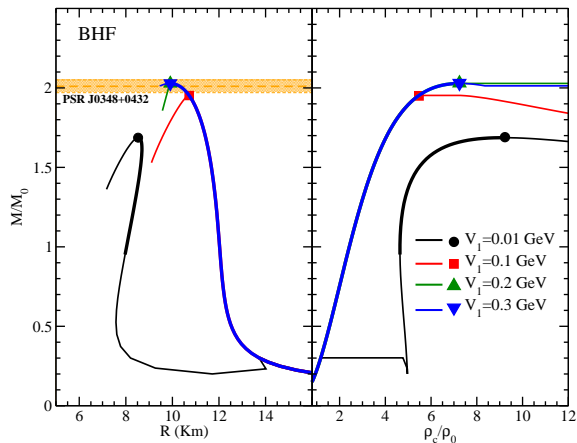


FIG. 5: The mass-radius (left panel) and the mass-central density relation (right panel) are displayed for different values of V_1 and the BHF hadronic EoS. The full symbols denote the value of the maximum mass. Stable configurations are displayed by thick lines, whereas thin lines indicate unstable configurations. G_2 is dependent on μ_B . (see text for details).

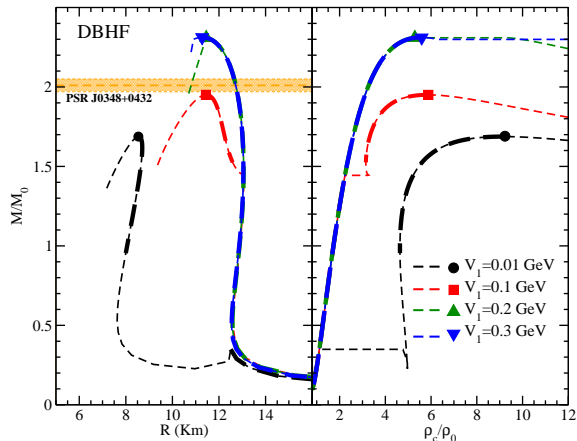


FIG. 6: Same as Fig.5 but with DBHF EoS used for the hadronic phase. The full symbols denote the value of the maximum mass. (see text for details).

is the largest value which produces stable neutron stars with a quark core.

Similar results are displayed in Fig.6, where the DBHF EoS is used for the hadronic phase, with the same notations and coding adopted in Fig. 5. Also in this case the observational data indicate that values of V_1 as small as 0.01 GeV are excluded, and that values of about 0.1 GeV are only marginally compatible with the observational data. This is due to the fact that for $V_1 = 0.1$ GeV the phase transition takes place over a range of densities where both BHF and DBHF EoS's show a similar behavior, but in the latter case a stable quark matter phase is produced, as can also be deduced from the asterisks reported in Table II.

By increasing the value of V_1 , the value of the maximum mass increases, but the stability of the pure quark

TABLE II: Properties of maximum mass configurations. Asterisks denote stable hybrid stars with pure quark matter core.

	V_1 (GeV)	M_{\max}/M_{\odot}	ρ_c/ρ_0	$G_2^c(\text{GeV}^4)$
BHF	0.01	1.69*	9.23	0.0042
	0.1	1.95	5.47	–
	0.2	2.03	7.24	–
	0.3	2.03	7.24	–
DBHF	0.01	1.69*	9.23	0.0042
	0.1	1.95*	5.88	0.0023
	0.2	2.31	5.29	–
	0.3	2.31	5.59	–

phase is lost, as shown in both Figs.5 and 6 by the cusps in the mass-radius relation, and the maximum mass contains in its interior at most a mixed quark-hadron phase. The maximum mass can increase well above the observational limit with increasing the value of V_1 , but hybrid stars will be mainly in the hadronic phase. We found that $V_1 \approx 0.12$ GeV is the largest value which produces stable neutron stars with a quark core if the DBHF EoS is used for the hadronic phase.

Therefore, generally speaking we can conclude that this model gives values of the maximum mass in agreement with the current observational data if $V_1 \gtrsim 0.1$ GeV. We remind the reader that those calculations have been performed assuming a dependence of the gluon condensate G_2 on the baryon chemical potential μ_B . For comparison, we show in Fig.7 the dependence of the maximum mass on the value of a constant G_2 , which was discussed in our previous paper [5]. There are some differences, mainly when a small value of $V_1 = 0.01$ GeV is used. In fact, in this case the value of the maximum mass is compatible with observational data only if a stiff EoS for the hadronic phase is adopted and, at the same time, sufficiently large values of G_2 are selected. With increasing V_1 , the value of the maximum mass increases, no matter the EoS for the hadronic phase, as already displayed in Figs. 5 and 6 with G_2 dependent on μ_B . Still, the BHF EoS is only marginally compatible with the data whereas the DBHF points lie well above the observed NS masses. We also notice that, already at $V_1 = 0.1$ GeV and more evidently at $V_1 = 0.2$ GeV, the values of M_{\max} collected in Fig. 7 are essentially independent of G_2 , thus indicating that the quark matter appears only after the hadronic branch has reached its maximum, M_{\max} , so that the corresponding star has no quark matter content.

VI. CONCLUSIONS

In this paper we have studied the effects of the appearance of a quark matter core in NS, with the corresponding quark-gluon EoS derived in the framework of the FCM and with a suitable parametrization of the gluon condensate in terms of the baryon chemical poten-

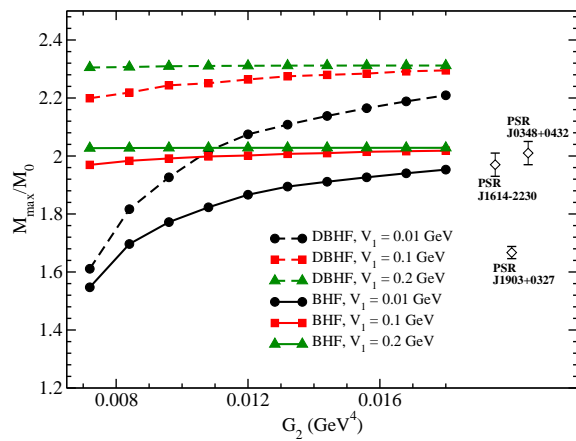


FIG. 7: The maximum mass, in units of the solar mass M_\odot , is displayed vs. the gluon condensate G_2 . G_2 is independent on μ_B .

tial, as suggested by the analysis of this variable for the theory with $N_c = 2$, where $G_2(\mu_B)$ turns out to be a decreasing function at small μ_B and increasing at larger μ_B . The inclusion of a density dependent gluon condensate is motivated by the expectations of some significant effect related to the onset of a superconductive phase at large density, which could be hidden by the use of a constant G_2 . Therefore, the absence of indications coming from lattice simulations at finite μ_B in the theory with $N_c = 3$, has forced us to resort to the only suggestion available on the behaviour of $G_2(\mu_B)$. Clearly these comments put some limits on the quantitative accuracy of the gluon condensate parametrization here adopted, which however should be regarded just as a qualitative description that could signal potential flaws of the simpler picture obtained by retaining constant G_2 .

The same kind of problem shows up for the other parameter entering the quark matter EoS, namely V_1 , that is expected to decrease when μ_B grows, because of the screening of the quark-antiquark interaction due to the increasing density. In this case we have no quantitative indication about its μ_B dependence, except for the suggestion, given in [11], that V_1 is substantially μ independent at least for $\mu \approx 0$. Therefore we performed our analysis at various constant values of the potential V_1 .

Our results are collected in Figs. 5 and 6 and Table II and they indicate that, with the adopted parametrization of $G_2(\mu_B)$, it is necessary to have $V_1 \gtrsim 0.1$ GeV in order to achieve $M_{\max} \approx 2M_\odot$. For larger V_1 , M_{\max} increases but no pure quark phase is present in the core of the NS already for $V_1 \gtrsim 0.12$ GeV and, beyond 0.3 GeV, M_{\max}

does not grow any more. Its value only depends on the particular hadronic EoS chosen. This picture is a substantial refinement of the results found in [5] where only vanishing or very small of V_1 were considered. In fact it was observed that M_{\max} grows both with V_1 and G_2 and in particular it was found $M_{\max} = 1.78M_\odot$ at constant $G_2 = 0.012$ GeV⁴ and $V_1 = 0.01$ GeV, which was consistent with the NS masses measured until then, but cannot explain the more recent measurements. In addition, in [5], the disappearance of the pure quark phase when increasing G_2 , was noticed as well.

Analogous results are also obtained in [21] for constant G_2 , but in this case larger values of M_{\max} are obtained because the chosen hadronic EoS, based on the relativistic mean field model, is considerably stiffer than the one adopted in this paper.

A final comment on the potential V_1 is in order. As already noticed, our analysis shows that the observed NS masses require values larger than 0.1 GeV while above 0.3 GeV the quark phase is no longer relevant in the determination of the maximum NS mass. These characteristic values of V_1 are much smaller than those coming from the analysis shown in Sec. II A on the lattice data at $\mu_B = 0$ around and above the critical temperature, which, when extrapolated to $T = 0$, yield $V_1(T = \mu_B = 0) = 0.8 \div 0.9$ GeV. This is to be taken as a clear indication that the long distance potential is indeed sensitive to the increase of density that induces a screening effect. However we also expect that when μ_B grows, the quark population increases with respect to the antiquark, so that the quark-quark interaction becomes more and more relevant, and eventually it is conceivable that it becomes predominant with respect to the quark-antiquark interaction. According to this point one could imagine to replace the singlet, V_1 , with the antitriplet, V_3 and sextet V_6 interactions, whose relative weights with respect to V_1 are respectively $(1/2)$ and $(-1/4)$. This leads to an effective interaction whose strength is about $(1/4)$ of the original one, $V_1(T = \mu_B = 0)$, so that this extremely simplified picture does nevertheless predict a value of the effective interaction at large baryon density (around 0.2 GeV), that is compatible with the relevant range of V_1 suggested by our analysis.

Acknowledgments

The authors warmly thank M. P. Lombardo (INFN-LNF) for enlightening discussions concerning the gluon condensate G_2 .

-
- [1] G. Taranto, M. Baldo, and G. F. Burgio, Phys. Rev. C **87**, 045803 (2013).
 [2] J. Antoniadis et al., Science **340**, (2013) 6131.
 [3] A. Di Giacomo, H.G. Dosch, V.I.Shevchenko, and Y.A.

- Simonov, Phys. Rep **372**, (2002) 319.
 [4] M. Baldo, G.F. Burgio, P. Castorina, S. Plumari, and D. Zappalà, Phys. Rev. C **75**, (2007) 035804.
 [5] M. Baldo, G.F. Burgio, P. Castorina, S. Plumari, and D.

- Zappalà, Phys. Rev. D **78**, (2008) 063009.
- [6] Yu.A. Simonov, Phys. Lett. B **619**, (2005) 293.
- [7] Yu.A. Simonov, and M.A. Trusov, JETP Lett. **85** (2007) 598.
- [8] Yu.A. Simonov, and M.A. Trusov, Phys. Lett. B **650** (2007) 36.
- [9] Yu.A. Simonov, Annals Phys. **323** (2008) 783.
- [10] E.V. Komarov, and Yu.A. Simonov, Annals Phys. **323** (2008) 1230.
- [11] A. V. Nefediev, Yu.A. Simonov, and M.A. Trusov, Int. J. Mod. Phys. E **18** (2009) 549.
- [12] M. Doring, S. Ejiri, O. Kaczmarek, F. Karsch, and E. Laermann, Eur. Phys. J. C **46** (2006) 179.
- [13] M.A. Shifman, A.I. Vainshtein, and V.I. Zakharov, Nucl. Phys. B **147** (1979) 385; Nucl. Phys. B **147** (1979) 448.
- [14] S. Borsanyi et al., JHEP **1009** (2010) 073.
- [15] S. Borsanyi et al., JHEP **1011** (2010) 077.
- [16] A. Bazavov et al., Phys. Rev. D **80** (2009) 014504.
- [17] A. Bazavov et al., Phys. Rev. D **85**, (2012) 054503.
- [18] USQCD Collaboration, C. De Tar and F. Karsch, "Computational Challenges in QCD Thermodynamics", <http://www.usqcd.org/documents/13thermo.pdf>
- [19] M. D'Elia, A. Di Giacomo, and E. Meggiolaro, Phys. Lett. B **408** (1997) 315.
- [20] M. D'Elia, A. Di Giacomo, and E. Meggiolaro, Phys. Rev. D **67** (2003) 114504.
- [21] I. Bombaci, and D. Logoteta, MNRAS **433** (2013) L79.
- [22] T. D. Cohen, R. J. Furnstahl, and D. K. Griegel, Phys. Rev. C **45** (1992) 1881.
- [23] E. G. Drukarev, M. G. Ryskin, and V. A. Sadovnikova, Prog. Part. Nucl. Phys. **47** (2001) 73.
- [24] M. Baldo, P. Castorina, and D. Zappalà, Nucl. Phys. A **743**, (2004) 3.
- [25] M. A. Metlitski, and A. R. Zhitnitsky, Nucl. Phys. B **731** (2005) 309.
- [26] A. R. Zhitnitsky, AIP Conf. Proc. **892** (2007) 518. ArXiv:hep-ph/0701065.
- [27] S. Hands, S. Kim, and J. I. Skullerud, Eur. Phys. J. C **48** (2006) 193.
- [28] B. Alles, M. D'Elia, and M. P. Lombardo, Nucl. Phys. B **752** (2006) 124.
- [29] M. Baldo, *Nuclear Methods and the Nuclear Equation of State*, International Review of Nuclear Physics, Vol. 8 (World Scientific, Singapore, 1999).
- [30] M. Baldo, I. Bombaci, and G. F. Burgio, Astron. Astrophys. **328**, (1997) 274; X. R. Zhou, G. F. Burgio, U. Lombardo, H.-J. Schulze, and W. Zuo, Phys. Rev. C **69**, (2004) 018801.
- [31] R. B. Wiringa, V. G. J. Stoks, and R. Schiavilla, Phys. Rev. C **51**, 38 (1995).
- [32] J. Carlson, V. R. Pandharipande, and R. B. Wiringa, Nucl. Phys. A **401**, 59 (1983); R. Schiavilla, V. R. Pandharipande, and R. B. Wiringa, Nucl. Phys. A **449**, 219 (1986).
- [33] W. D. Myers and W. J. Swiatecki, Nucl. Phys. A **601**, 141 (1996); Phys. Rev. C **57**, 3020 (1998).
- [34] T. Gross-Boeltling, C. Fuchs, and A. Faessler, Nucl. Phys. A **648**, 105 (1999).
- [35] G. E. Brown, W. Weise, G. Baym, and J. Speth, Comments Nucl. Part. Phys. **17**, 39 (1987).
- [36] H.-J. Schulze, A. Lejeune, J. Cugnon, M. Baldo, and U. Lombardo, Phys. Lett. B **355**, (1995) 21; H.-J. Schulze, M. Baldo, U. Lombardo, J. Cugnon, and A. Lejeune, Phys. Rev. C **57**, (1998) 704.
- [37] M. Baldo, G. F. Burgio, and H.-J. Schulze, Phys. Rev. C **58**, (1998) 3688; Phys. Rev. C **61**, (2000) 055801.
- [38] S.L. Shapiro and S.A. Teukolsky, *Black Holes, White Dwarfs and Neutron Stars* (John Wiley and Sons, New York, 1983).
- [39] Z. Fodor and S. D. Katz, JHEP **0404** (2004) 050.
- [40] N. K. Glendenning, *Compact Stars, Nuclear Physics, Particle Physics, and General Relativity*, 2nd ed. (Springer, New York, 2000).
- [41] T. Endo, T. Maruyama, S. Chiba, and T. Tatsumi, Prog. Theor. Phys. **115**, (2006) 337.
- [42] G. F. Burgio, M. Baldo, P. K. Sahu, A. B. Santra, and H.-J. Schulze, Phys. Lett. B **526**, (2002) 19; G. F. Burgio, M. Baldo, P. K. Sahu, and H.-J. Schulze, Phys. Rev. C **66**, (2002) 025802.
- [43] J. W. Negele, and D. Vautherin, Nucl. Phys. A **207**, (1973) 298.
- [44] G. Baym, C. Pethick, and D. Sutherland, Astrophys. J. **170**, (1971) 299.
- [45] R. Feynman, F. Metropolis, and E. Teller, Phys. Rev. C **75**, (1949) 1561.